From FEM to MBS: Stability Analysis of the Elastic H/C-Rotor

Stefan Waitz

Institute of Aeroelasticity, DLR, Göttingen, Germany

Abstract

As a consequence of the variety of effects the rotation has on the vibrating structure it is important to take into account the complete shares of the gyroscopic influence in the equation of motion. One prerequisite will be the formulation of the mass terms for all three axis of rotational movement of the vibrating rotor even if it deals with slender beam like structures. This is the case as well in the in-house Finite Element Method code GYRBLAD (FEM) as in the commercial Multi Body System code SIMPACK (MBS), which both have been applied in this investigation. The numerical calculations of the eigenmodes and the stability behaviour of the rotor will be conducted by using two different modelling concepts: the advantage of the FEM code lies in the capability of describing the deformation of a flexible structure in an already linearised manner (Euler-Bernoulli beam), whereas the potential of the MBS code comes from the complete nonlinear formulation of the arbitrarily large movements of elastically interacting (rigid) bodies in an equilibrium or accelerated state. In order to take into account the characteristics of the flexible continuum also in MBS the code offers the special feature FEMBS for combining the FEM with MBS modelling. Thus the potential of a sophisticated, hybrid MBS code like SIMPACK as a powerful simulation tool for helicopter dynamics will be demonstrated with respect to the dynamics of the elastic rotor.

For validation purpose the results of the FEM and the MBS code are quantitatively compared to the results of the analytical description of the dynamic behaviour of the rigid body rotor. Representing the case of fixed boundary conditions at a rigid hub the results of a single rotating blade are shown. The Princeton beam with its double symmetric cross section allows the focus on the DOF coupling as a result only from the rotation. For a single blade the pure gyroscopic coupling will be displayed for the flapping-torsion and the lagging-stretching movement. The investigation of the complete rotor (four and six blades) follows where all classes of rotor eigenmodes (collective, cyclic and reactionless) will be studied. As results for the eigenbehaviour the coupled complex eigenmodes and the variation of the eigenfrequencies with respect to the rotation speed will be shown (fan diagrams). Resonance phenomena in the eigenmodes occur at specific rotor speeds and frequencies where the pitch (torsion) amplitude rises over all measures. Although slim and slender bodies with a high aspect ratio are investigated not negligible coupling effects specially on the blade pitch movement have to be stated. For the aeroelastic stability analysis of the rotating elastic helicopter blade this can be highly hazardous.

1 Introduction

The rotational movement of the rotor blades of a helicopter in operation subjects the blade and hub structure to rotation specific loads which in general are very high and thus potentially operation limiting constraints. These acceleration effects are specially rotor speed dependent and may not be neglected in a dynamic simulation analysis under any circumstance. The gyroscopic effects have an essential impact on the elastic blade and the complete H/C-rotor and influence their vibration behaviour significantly. Eigenfrequencies and eigenmodes can change totally their amount and shape with respect to the rotation speed.

In a linear dynamic analysis the gyroscopic effects have to be superimposed to the "original" dynamic behaviour which is displayed by the blade structure already in the non-rotating state. For the computation of large deformation states high performance (geometric) non-linear codes have to be applied. In recent time Multi Body System (MBS) codes have found their way into structural analysis within the helicopter industry and the use of commercial MBS tools in the general design and developpement process seems to become common.

These MBS codes combine their inherent property of describing large deflections of the (rigid) structure including full geometric non-linearities with in general high performance time integration algorithms. In combination with special algorithmic features Finite Element Model (FEM) substructures can be incorporated into the MBS model replacing one or several rigid body components. By applying these so called FEMBS techniques consistent elastic properties can be introduced into the structure to any desired amount. Together with these FEMBS structures and additional degrees of freedom added to the hybrid MBS model the total dynamic model can be subjected to any kind of numerical simulation. Thus with MBS and FEM two fundamentally different approaches in structural dynamics can be combined with their respective advantages to potential high power CSD tools.

Since the most MBS codes have not primarily been designed for describing rotating elastic helicopter blades with their numerous potentially coupling mechanisms, in this paper these special features have been subjected to a systematic investigation to verify their correctness and reliability. It could be shown that one potential drawback of the MBS approach — the composition of the system matrices in a linearised equation of motion for the consecutive eigenvalue analysis — is succsessfully tackled with due to high performance differentiating algorithms.

In this paper the commercial MBS code SIMPACK has been validated by comparisons to the FEM code GYRBLAD. Our own in-house code GYRBLAD has primarily been designed for rotating 3-D beam like structures and contains the complete gyroscopic terms necessary to describe the spacial movement of a rotating elastic structure. Additional comparisons have been done to the commercial FEM tool NASTRAN and to exact solutions from linearised analytical models.

The effort to keep a low error margin in the results to be compared proved to be successful. Most of the eigenvalue results show a relative error of around 0.1%. To reach values further below this margin would have needed an additional high numerical effort in model resolution. On the other hand error margins approaching or passing the 1% margin would have been a sign for wrong or incomplete modelling — on either of both sides to be compared.

2 The Princeton beam

Since in this investigation the focus was put on the gyroscopic effects of the rotating structure the so called "Princeton beam" had been chosen as the generic elastic rotor beam. The original Princeton beam had been submitted to wide experimental testing and the results have been published in [1]. With its double symmetric cross section any stiffness or mass coupling is excluded a priori and it is guaranteed for that a coupling between the various degrees of freedom in case of rotation originates only from the gyroscopic effects.

The original Princeton beam had a length of 20 [in] and a cross section of 0.5×0.125 [in^2]. Because of

the aim of describing and validating the coupling of all possible DOF combinations a structural system had to be found where the longitudinal eigenmodes — at least one — lie sufficient low in the range of the system eigenvalues. That is why for the numerical investigation here the length of the beam has been enlarged to 8 [m] and — by preserving the aspect ratios of the Princeton beam — the cross section was widened to 0.2 x 0.05 [m^2]. Thus a model beam had been created which has the same material values and the same aspect ratios as the original Princeton beam but which is ∼16 times enlarged in the external dimensions. The system values of this modified Princeton beam are defined as following:

$$l = 8.0\ [\text{m}]\ ;\ b = 0.20\ [\text{m}]\ ;\ h = 0.05\ [\text{m}]\ ;$$
$$l/b = 40\ [\text{-}]\ ;\ b/h = 4\ [\text{-}]\ ;$$
$$E = 71.73 * 10^9\ [\text{N/m}^2]\ ;\ G = 26.90 * 10^9\ [\text{N/m}^2]\ ;$$
$$\nu = 0.33\ [\text{-}]\ ;\ \rho = 2796.\ [\text{kg/m}^3]\ ;\ \eta = 0.843\ [\text{-}]$$

The first 17 eigenfrequencies of the modified elastic Princeton beam w/r to rotor speed are shown in the fan diagramm (Fig. 1). There it can be seen that within the range of 160 [Hz] the first 17 eigenmodes comprise 2 torsional (43 and 130 [Hz]) and one elongation mode (158 [Hz]) (index letters "T" and "X") as well as 5 lagging and 9 flapping modes (index letters "Y" and "Z") (see also Tab. 7 and 9).

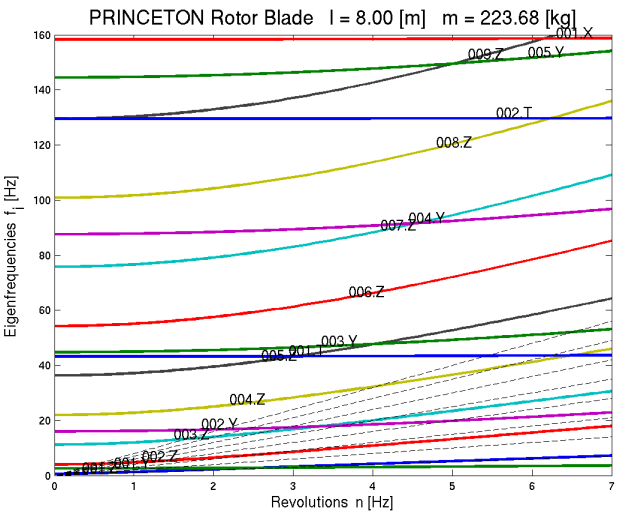

Figure 1: The single blade: The first 17 eigenfrequencies w/r to rotor speed (GYRBLAD)

3 Modelling with MBS

Within a MBS algorithm the equations of motion in general are capable of describing in a non-linear formulation arbitrarily large displacements of the individual rigid bodies which in turn are designed for three-dimensional movement. This implies that on one hand the complete mass tensor, crucial for capturing the gyroscopic effects, is included in the simulation model. On the other hand there is the need to linearise the equations of motion prior to carrying out a stability analysis. The linearisation process which is obsolete in an a priori linearised and balanced Finite Element model requires high fidelity linearisation and equilibrating algorithms. The eigenvalue results compared in this study showed to be quite sensitive to the respective algorithm and the accuracy of the linearisation process.

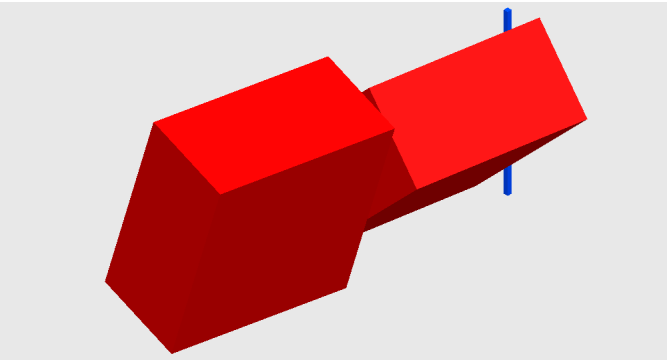

Figure 2: The rigid double pendulum: The second coupled flapping-torsion eigenmode (with f=1.2517[Hz], n=0.8[Hz]) (SIMPACK)

As an exampel for a simple but complete two body MBS system a double pendulum rotating around the vertical axis is presented and here its eigenbehaviour has been investigated by three different methods (two eigenmodes to be seen in Fig. 2 and 3). Each of the two bodies owns three-dimensional mass properties and originally the six DOF for the description of movement in space. The force interaction between the two bodies as well as between the inner body and the rotation axis (hub) takes place by means of the stiffness of the applied springs. For reasons of compatibility the two x two lateral DOF v_i and w_i are blocked and thus this sys-

The System Mass Matrix:

$$\left[\underline{M}_s\right] = \begin{bmatrix} m & \frac{m}{2} & 0 & 0 & 0 & 0 & 0 & 0 \\ \frac{m}{2} & \frac{m}{2} & 0 & 0 & 0 & 0 & 0 & 0 \\ 0 & 0 & m\left(\frac{l_g^2}{4}+\frac{l_g^2+b^2}{12}\right) & \frac{m}{2}\left(\frac{l_k^2}{4}+\frac{l_k^2+b^2}{12}\right)+\frac{m}{2}\left(\frac{l_g}{2}\right)\left(\frac{l_k}{2}\right) & 0 & 0 & 0 & 0 \\ 0 & 0 & \frac{m}{2}\left(\frac{l_k^2}{4}+\frac{l_k^2+b^2}{12}\right)+\frac{m}{2}\left(\frac{l_g}{2}\right)\left(\frac{l_k}{2}\right) & \frac{m}{2}\left(\frac{l_k^2}{4}+\frac{l_k^2+b^2}{12}\right) & 0 & 0 & 0 & 0 \\ 0 & 0 & 0 & 0 & m\left(\frac{h^2+b^2}{12}\right) & \frac{m}{2}\left(\frac{h^2+b^2}{12}\right) & 0 & 0 \\ 0 & 0 & 0 & 0 & \frac{m}{2}\left(\frac{h^2+b^2}{12}\right) & \frac{m}{2}\left(\frac{h^2+b^2}{12}\right) & 0 & 0 \\ 0 & 0 & 0 & 0 & 0 & 0 & m\left(\frac{l_g^2}{4}+\frac{h^2+l_g^2}{12}\right) & \frac{m}{2}\left(\frac{l_k^2}{4}+\frac{h^2+l_k^2}{12}\right)+\frac{m}{2}\left(\frac{l_g}{2}\right)\left(\frac{l_k}{2}\right) \\ 0 & 0 & 0 & 0 & 0 & 0 & \frac{m}{2}\left(\frac{l_k^2}{4}+\frac{h^2+l_k^2}{12}\right)+\frac{m}{2}\left(\frac{l_g}{2}\right)\left(\frac{l_k}{2}\right) & \frac{m}{2}\left(\frac{l_k^2}{4}+\frac{h^2+l_k^2}{12}\right) \end{bmatrix};$$

Table 1: The rigid double pendulum: The system mass matrix

The Geometric Stiffness Matrix:

$$\left[\underline{K}_g\right] = \begin{bmatrix} 0 & 0 & 0 & 0 & 0 & 0 & 0 & 0 \\ 0 & 0 & 0 & 0 & 0 & 0 & 0 & 0 \\ 0 & 0 & m\left(0+\frac{l_g}{2}\right)\left(\frac{l_g}{2}\right) & \frac{m}{2}\left(l_k+\frac{l_k}{2}\right)\left(\frac{l_k}{2}\right) & 0 & 0 & 0 & 0 \\ 0 & 0 & \frac{m}{2}\left(l_k+\frac{l_k}{2}\right)\left(\frac{l_k}{2}\right) & \frac{m}{2}\left(l_k+\frac{l_k}{2}\right)\left(\frac{l_k}{2}\right) & 0 & 0 & 0 & 0 \\ 0 & 0 & 0 & 0 & 0 & 0 & 0 & 0 \\ 0 & 0 & 0 & 0 & 0 & 0 & 0 & 0 \\ 0 & 0 & 0 & 0 & 0 & 0 & m\left(0+\frac{l_g}{2}\right)\left(\frac{l_g}{2}\right) & \frac{m}{2}\left(l_k+\frac{l_k}{2}\right)\left(\frac{l_k}{2}\right) \\ 0 & 0 & 0 & 0 & 0 & 0 & \frac{m}{2}\left(l_k+\frac{l_k}{2}\right)\left(\frac{l_k}{2}\right) & \frac{m}{2}\left(l_k+\frac{l_k}{2}\right)\left(\frac{l_k}{2}\right) \end{bmatrix};$$

Table 2: The rigid double pendulum: The geometric stiffness matrix

The System Stiffness Matrix:

$$\left[\underline{K}_s\right] = \begin{bmatrix} c_1 & 0 & 0 & 0 & 0 & 0 & 0 & 0 \\ 0 & c_1 & 0 & 0 & 0 & 0 & 0 & 0 \\ 0 & 0 & \widehat{c_6} & 0 & 0 & 0 & 0 & 0 \\ 0 & 0 & 0 & \widehat{c_6} & 0 & 0 & 0 & 0 \\ 0 & 0 & 0 & 0 & \widehat{c_4} & 0 & 0 & 0 \\ 0 & 0 & 0 & 0 & 0 & \widehat{c_4} & 0 & 0 \\ 0 & 0 & 0 & 0 & 0 & 0 & \widehat{c_5} & 0 \\ 0 & 0 & 0 & 0 & 0 & 0 & 0 & \widehat{c_5} \end{bmatrix};$$

Table 3: The rigid double pendulum: The system stiffness matrix

The Centrifugal Stiffness Matrix:

$$\left[\,\underline{K}_f\,\right] = \begin{bmatrix} m & \frac{m}{2} & 0 & 0 & 0 & 0 & 0 & 0 \\ \frac{m}{2} & \frac{m}{2} & 0 & 0 & 0 & 0 & 0 & 0 \\ 0 & 0 & m\left(\frac{l_g}{2}\right)^2 & \frac{m}{2}\left(\frac{l_k}{2}\right)\left(\frac{l_g+l_k}{2}\right) & 0 & 0 & 0 & 0 \\ 0 & 0 & \frac{m}{2}\left(\frac{l_k}{2}\right)\left(\frac{l_g+l_k}{2}\right) & \frac{m}{2}\left(\frac{l_k}{2}\right)^2 & 0 & 0 & 0 & 0 \\ 0 & 0 & 0 & 0 & m\left(\frac{h^2-b^2}{12}\right) & \frac{m}{2}\left(\frac{h^2-b^2}{12}\right) & 0 & 0 \\ 0 & 0 & 0 & 0 & \frac{m}{2}\left(\frac{h^2-b^2}{12}\right) & \frac{m}{2}\left(\frac{h^2-b^2}{12}\right) & 0 & 0 \\ 0 & 0 & 0 & 0 & 0 & 0 & m\left(\frac{h^2-l_g^2}{12}\right) & \frac{m}{2}\left(\frac{h^2-l_k^2}{12}\right) \\ 0 & 0 & 0 & 0 & 0 & 0 & \frac{m}{2}\left(\frac{h^2-l_k^2}{12}\right) & \frac{m}{2}\left(\frac{h^2-l_k^2}{12}\right) \end{bmatrix} ;$$

Table 4: The rigid double pendulum: The centrifugal stiffness matrix

The Gyroscopic Matrix:

$$\left[\,\underline{D}_g\,\right] = \begin{bmatrix} 0 & 0 & -m\left(\frac{l_g}{2}\right) & -\frac{m}{2}\left(\frac{l_k}{2}\right) & 0 & 0 & 0 & 0 \\ 0 & 0 & -\frac{m}{2}\left(\frac{l_g+l_k}{2}\right) & -\frac{m}{2}\left(\frac{l_k}{2}\right) & 0 & 0 & 0 & 0 \\ m\left(\frac{l_g}{2}\right) & \frac{m}{2}\left(\frac{l_g+l_k}{2}\right) & 0 & 0 & 0 & 0 & 0 & 0 \\ \frac{m}{2}\left(\frac{l_k}{2}\right) & \frac{m}{2}\left(\frac{l_k}{2}\right) & 0 & 0 & 0 & 0 & 0 & 0 \\ 0 & 0 & 0 & 0 & 0 & 0 & -m\left(\frac{h^2}{12}\right) & -\frac{m}{2}\left(\frac{h^2}{12}\right) \\ 0 & 0 & 0 & 0 & 0 & 0 & -\frac{m}{2}\left(\frac{h^2}{12}\right) & -\frac{m}{2}\left(\frac{h^2}{12}\right) \\ 0 & 0 & 0 & 0 & m\left(\frac{h^2}{12}\right) & \frac{m}{2}\left(\frac{h^2}{12}\right) & 0 & 0 \\ 0 & 0 & 0 & 0 & \frac{m}{2}\left(\frac{h^2}{12}\right) & \frac{m}{2}\left(\frac{h^2}{12}\right) & 0 & 0 \end{bmatrix} ;$$

Table 5: The rigid double pendulum: The gyroscopic matrix

RIGID DOUBLE PENDULUM (l/b/h = 8/4/2 [m])

	ANALYTICAL 8 DOF	GYRBLAD (FEM) 8 Elem.		SIMPACK (MBS) 2 Bodies		
	0.8740 [Hz]	0.8740 [Hz]	.00 [%]	0.8740 [Hz]	.00 [%]	- Elgn.
n =	0.8740 [Hz]	0.8740 [Hz]	.00 [%]	0.8740 [Hz]	.00 [%]	- Trsn.
.0 [Hz]	0.9524 [Hz]	0.9524 [Hz]	.00 [%]	0.9524 [Hz]	.00 [%]	- Flap.
	0.9497 [Hz]	0.9497 [Hz]	.00 [%]	0.9497 [Hz]	.00 [%]	- Lagg.
	0.1913 [Hz]	0.1913 [Hz]	.00 [%]	0.1914 [Hz]	.05 [%]	- Elgn.
n =	1.0600 [Hz]	1.0599 [Hz]	-.01 [%]	1.0600 [Hz]	.00 [%]	- Trsn.
.8 [Hz]	1.2517 [Hz]	1.2522 [Hz]	.04 [%]	1.2517 [Hz]	.00 [%]	- Flap.
	1.6772 [Hz]	1.6775 [Hz]	.02 [%]	1.6773 [Hz]	.01 [%]	- Lagg.

Table 6: The eigenfrequencies of the rotating/non-rotating rigid double pendulum (three methods ANALYTICAL, FEM, MBS; errors related to the ANALYTICAL solution)

tem rotating with steady speed owns eight DOF in total.

The complete linearised equation of motion for the rotating system in general discretised degrees of freedom reads (for the MBS as well as for the FEM formulation):

$$\left(\left[\underline{K}_s \right] - \Omega^2 \left[\underline{K}_f \right] + \Omega^2 \left[\underline{K}_g \right] \right) \left\{ \underline{u} \right\} + \\ + 2\Omega \left[\underline{D}_g \right] \left\{ \underline{u} \right\}^{\cdot} + \left[\underline{M}_s \right] \left\{ \underline{u} \right\}^{\cdot\cdot} = \left\{ \underline{0} \right\} \quad (1)$$

In the Tabs. 1 until 5 the system matrices are displayed as a result of an analytical description. Here the MBS system matrices were built together in an a priori linearised manner. They comprise both the "classical" mass, damping and stiffness matrices of the linear dynamical system and additionally the rotation dependent gyroscopic terms. The respective DOF are distributed in the deflection vector of the double pendulum in the following order:

$$\left\{ \underline{u} \right\} = \left\{ u_1, u_2, \gamma_1, \gamma_2, \alpha_1, \alpha_2, \beta_1, \beta_2 \right\}^{\mathrm{T}} \quad (2)$$

This complete rotating system is now subjected to an eigenvalue algorithm and the resulting "exact" eigenfrequencies are compared to the numerical results achieved with two other methods: On one hand the linearised MBS system of SIMPACK and on the other hand the FEM calculations with the code GYRBLAD. The latter was adopted in a way that made it possible to simulate the "MBS behaviour" by introducing an artifical stiffening and additional joint-specific degrees of freedom. The values of the first four eigenfrequencies determined with the three methods are shown in Tab. 6 for the rotating as well as for the non-rotating system. The displayed error margins are related to the analytical system and lie in the lower permille range.

The appearing gyroscopic effects can be classified not only formally as contributions to the damping (antisymmetric matrix) and the stiffness terms (with either stiffening or softening impact) but also physically as phenomena which arise either from the deformation of the vibrating structure or the radius dependent position along the rotating blade (geometric stiffness). The impact of the gyroscopic terms on the

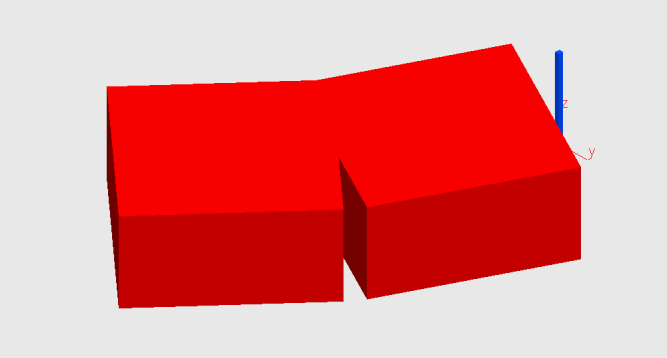

Figure 3: The rigid double pendulum: The second coupled lagging-elongation eigenmode (with f=1.6772[Hz], n=0.8[Hz]) (SIMPACK)

dynamic behaviour of the structure in general can be described as a coupling of (previously uncoupled) degrees of freedom. The eigenmodes — even of an originally undamped system — become complex and the eigenfrequencies will either be lifted or lowered. In the case of the presence of double eigenfrequencies ("1K"-modes; see below) previously equal frequencies will be split up. All these physical phenomena hold as well for the rotating rigid body models as for the elastic structure of a continuosly flexible rotor. (A suitable object for studying the gyroscopic phenomena is the rigid gyroscope of course.)

4 Modelling with FEM

As a consequence of the variety of the effects the rotation has on the vibrating structure it is important to take into account the complete shares of the gyroscopic influence in the equation of motion, e.g. for all DOF. One prerequisite will be the formulation of the mass terms of the vibrating rotor for all three axis of rotational movement even if it "only" deals with the slender, beam like structure of the rotor blades. As a matter of fact consistent mass distribution is required (in lumped mass modelling often the rotatory DOF is not included in the finite element formulation).

All this is the case as well in our in-house Finite Element code GYRBLAD (FEM) as in the commercial Multi Body System code SIMPACK (MBS), which both have been applied in the numerical calculations for the fully elastic blade. In order to take

into account the characteristics of the flexible continuum also in SIMPACK, the special feature of the MBS code for the combining of FEM and MBS modelling (= FEMBS) can be used. The modelling quality of the imported flexible Finite Element components is then dependent of the capabilities of the underlying FEM source.

Based on the common assumptions of the Euler-Bernoulli beam theory the deflection state can be split into two parts and the Finite Element formulation can be done seperately for the rotational and the translational displacements. In a virtual energy formulation the rotation depending additional terms look like:

$$\begin{aligned}\delta W_\Omega = 2\Omega \sum_i \int_{l_i} \mu_x \left(\delta u\, \dot{v} - \delta v\, \dot{u}\right) dx + \\ +2\Omega \sum_i \int_{l_i} \widehat{\mu}_h \left(\delta\alpha\, \dot{\beta} - \delta\beta\, \dot{\alpha}\right) dx - \\ -\Omega^2 \sum_i \int_{l_i} \mu_x \left(\delta u\, u + \delta v\, v\right) dx - \\ -\Omega^2 \sum_i \int_{l_i} \widehat{\mu}_h \left(\delta\alpha\, \alpha + \delta\beta\, \beta\right) dx + \\ +\sum_i \int_{l_i} N_x(\Omega) \left(\delta w'\, w' + \delta v'\, v'\right) dx \qquad (3)\end{aligned}$$

Since these in general so called gyroscopic effects appear not only linearly dependent of the rotor speed but also contribute quadratically speed-dependent terms to the equation of motion, their influence on the dynamic behaviour of the blades rises significantly with the rotor speed. They even represent the dominant parameters of the eigenbehaviour (eigenmodes and -frequencies) of the rotor structure in the various operating regimes of a helicopter.

An exampel for the normal forces in the blade due to rotation induced centrifugal accelerations is shown in Fig. 4. These normal forces are an integral part of the geometric stiffness matrix and have therefore to be determined in calculations in advance.

5 The single blade

Representing the case of fixed boundary conditions at a rigid hub the results for the clamped rotating single blade are shown. For various methods

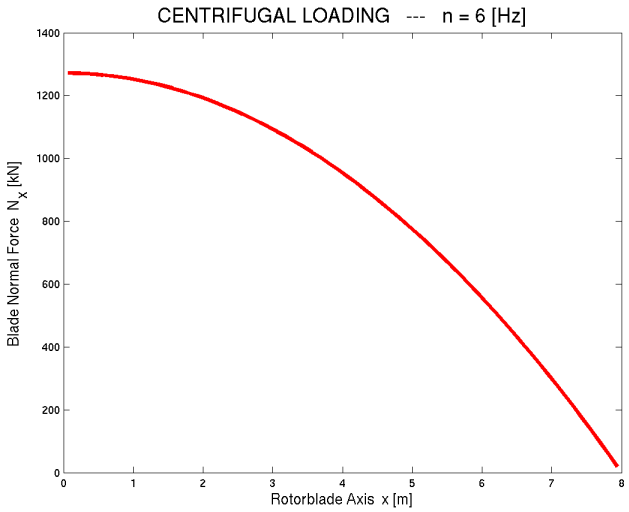

Figure 4: The blade axial force N_x of the 64 Finite Element Princeton beam at n=6[Hz] (GYRBLAD)

comparisons of the eigenvalues of the blade rotating at different speeds have been done. The pure gyroscopic coupling in the flapping-torsion and the lagging-stretching movement will become obvious by looking at the eigenmodes of the blade. The modified Princeton beam has been the generic blade which had been chosen as the object for the realisation of the calculations. In contrast to a technological unsymmetric blade the double symmetric cross section of the Princeton beam was of advantage because it allows the focus on the DOF coupling as a result only from the rotation. All other possible coupling mechanisms of an arbitrary real structure are excluded: coupling by mass, stiffness or aerodynamic effects — which on their part of course can influence the behaviour of the vibrating real rotor blades to a remarkable extent.

Thus the numerical calculations of the eigenmodes and the stability behaviour of the rotor have been conducted by using two different modelling concepts: the advantage of the FE code lies in the capability of describing the deformation of a flexible structure in an already linearised manner (Euler-Bernoulli beam), whereas the potential of the MBS code emerges from the complete nonlinear formulation of the arbitrarily large movements of elastically interacting (rigid) bodies in a equilibrium or acceleration state. The numerical models comprised 32

finite elements, 32 rigid bodies connected by discrete equivalent springs or one body FEMBS component respective.

As result of the calculations for the rotating and the non-rotating Princeton beam the eigenvalues for the lower 17 eigenmodes (9 flapping, 5 lagging, 2 torsion and 1 elongation mode) are displayed (see Tab. 7 and 9). The three above mentioned methods had been applied and their relative error margings (related to the GYRBLAD results) remain in the lower permille range. As to the hybrid FEMBS modelling a NASTRAN finite element model of the elastic Princeton beam was used to be incorporated into the SIMPACK rigid body formulation. One minor drawback of the NASTRAN beam in this case had been that it did not contain the rotatory mass terms. This explains the growing differences in the eigenfrequencies of the higher lagging modes (for the fifth lagging mode around 1%). The pure MBS model built up with 32 rigid bodies shows a slightly better performance than the FEMBS formulation except for the high flapping modes of the rotating sample where the error also reaches the 1% margin. There the model resolution of the 32 rigid bodies proved to be unsufficient for mapping higher modes (with around 9 nodes and more).

In the fan diagrams of Fig. 1 and 5 the eigenfrequencies of the Princeton beam are shown with respect to the rotation speed of the rotor axis resulting from GYRBLAD computations. In Fig. 5 additionally displayed are the results from several distinct SIMPACK calculations (marked with an "x" sign). It can be seen that the SIMPACK results lie well on the GYRBLAD curves. In Fig. 10 and 11 and Fig. 13 and 14 four eigenmodes at different rotating speeds are shown, each one for a different "main" deflection component being dominant. (For the purpose of easier analysing of the eigenmodes the GYRBLAD results have been displayed in four separated subdiagrams for the main component of the nodal displacements each.) Although the composition of every eigenmode changes with the rotation speed to take shape in any order the main characteristics of the gyroscopic coupling here clearly can be observed in the time delayed coupling of the DOF classes "flapping-torsion" and "lagging-stretching". The stereoscopic illustration of the respective eigenmodes can be seen in Fig. 9 and 12.

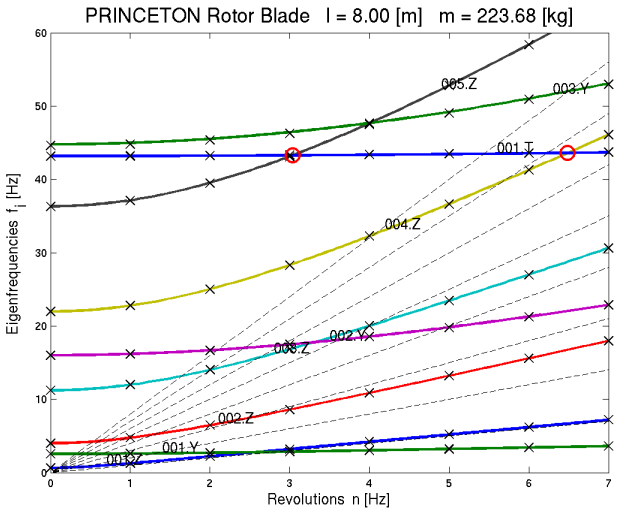

Figure 5: The single blade: The lower eigenfrequencies w/r to rotor speed (o = gyroscopic resonance) (GYRBLAD; x = SIMPACK)

6 The gyroscopic resonance

The rotation of the elastic blade causes a coupling between the components of the eigenvectors which — in case of the double symmetric cross section — in the non-rotating state have been uncoupled. Although with increasing rotor speed the coupling effect gets stronger the time delayed imaginary fraction of the eigenmodes remain relatively small as long as the blade is built up by a long and slender beam. Looking at the variation of the eigenmodes with increasing rotor speed ("Campbell diagrams for the eigenmodes") mode specific regions can be detected where the gyroscopically coupled components display a steep rise. Exceeding the nominal components they strive to infinity and — after changing sign — they attenuate again. These astonishing resonance-like effects in the eigenmodes occur at specific rotor speeds and frequencies between the gyroscopically coupled components.

In Fig. 5 two resonance areas at the crossing points of the first torsion with two flapping modes (the fourth and the fifth) are marked with orange circles. Looking at the component amplitudes of the

involved eigenmodes (see Fig. 7, 8, 6) one can not only perceive the distinct resonance points; it also is evident that in the adjacent frequency regions before and behind the resonance points an intense coupling with large coupled component fractions occur. Another example can be found at the crossing of the fifth lagging with the first elongation mode (see Fig. 1 in extrapolation). For the latter case and the lower one out of the two flapping/torsion cases the eigenmodes at rotor speeds in the neighbourhood of the respective resonance points are displayed in Fig. 9 and 12 from SIMPACK and in Fig. 10 and 11 and Fig. 13 and 14 from GYRBLAD calculations. In the SIMPACK pictures the spacial movement of the oscillating blade is captured whereas in the GYRBLAD diagrams the equal magnitude of the gyrosciopicly coupled DOF gets evident.

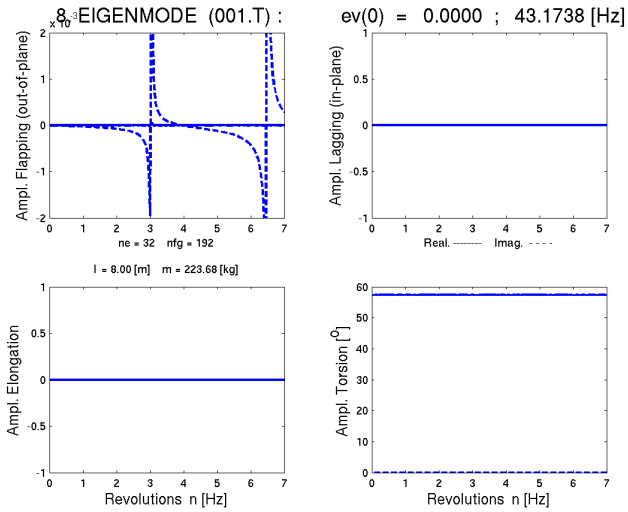

Figure 6: The single blade: Component amplitudes of the first torsion eigenmode w/r to rotor speed (GYRBLAD)

Concearning the blade aerodynamics especially the torsional movement is highly relevant. While the aerodynamic forces are sensitive already to minor changes of the pitch angles in the gyroscopic resonance areas the blade pitch amplitude rises over all measures. (At least the frequency bands of rotor speed of such areas are well confined.) Even for the slim and slender beam with high aspect ratio that has been investigated here — and how H/C blades use to be like — this effect is potentially dangerous with respect to the coupled flapping/torsional movement and the role it plays in aeroelastic stability. Although a real aeroelastic rotor system contains several other mass or stiffness coupling effects not negligible gyroscopic coupling especially on the blade pitch movement has to be stated. For the aeroelastic stability analysis of the rotating elastic helicopter blades these rotational effects can mean a favourable, i.e. damping, or a highly exciting influence.

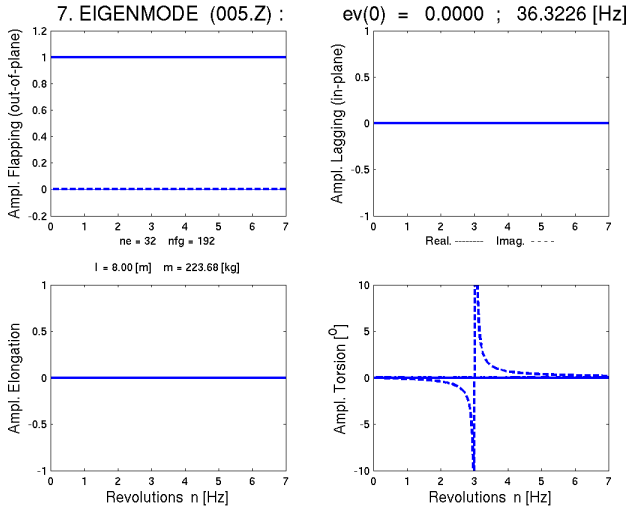

Figure 7: The single blade: Component amplitudes of the fifth flapping eigenmode w/r to rotor speed (GYRBLAD)

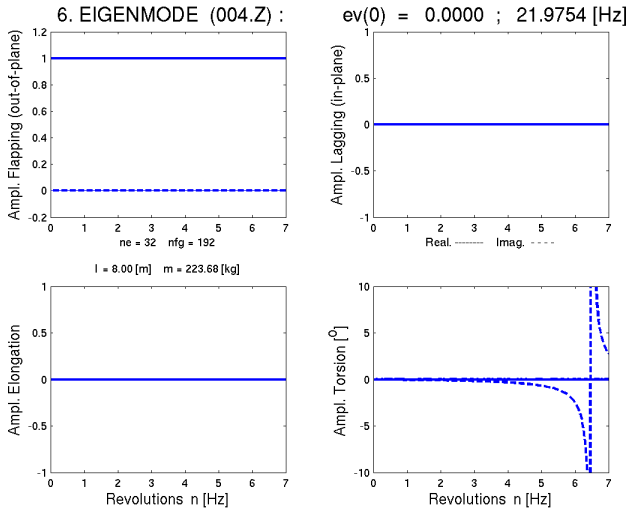

Figure 8: The single blade: Component amplitudes of the fourth flapping eigenmode w/r to rotor speed (GYRBLAD)

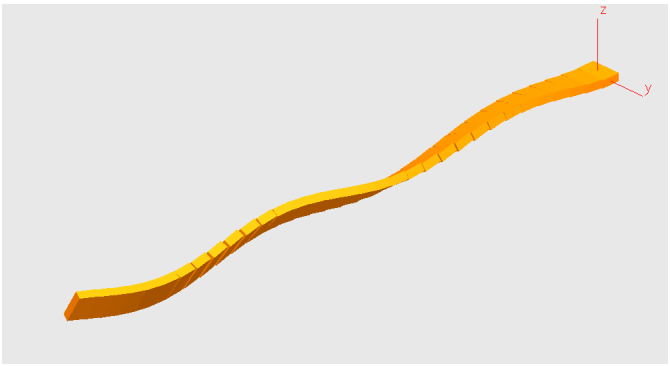

Figure 9: The single blade: The fifth flapping eigenmode at n=3.02[Hz] (SIMPACK)

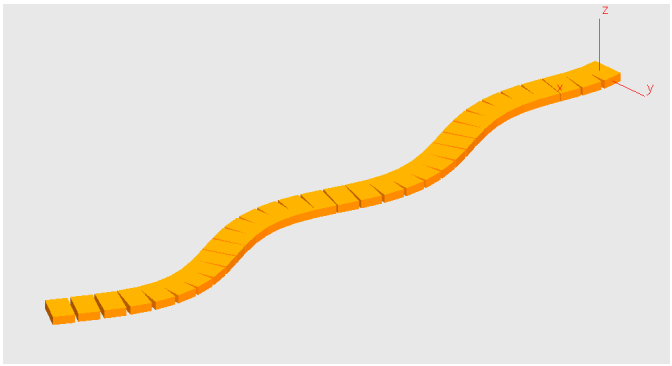

Figure 12: The single blade: The fifth lagging eigenmode at n=9.15[Hz] (SIMPACK)

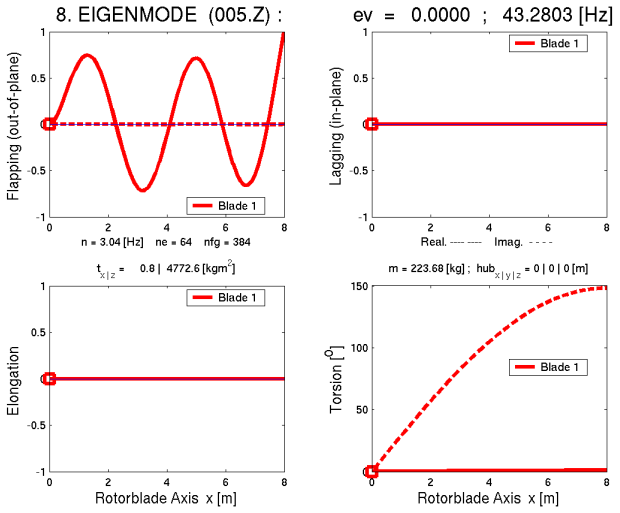

Figure 10: The single blade: The fifth flapping eigenmode at n=3.04[Hz] (GYRBLAD)

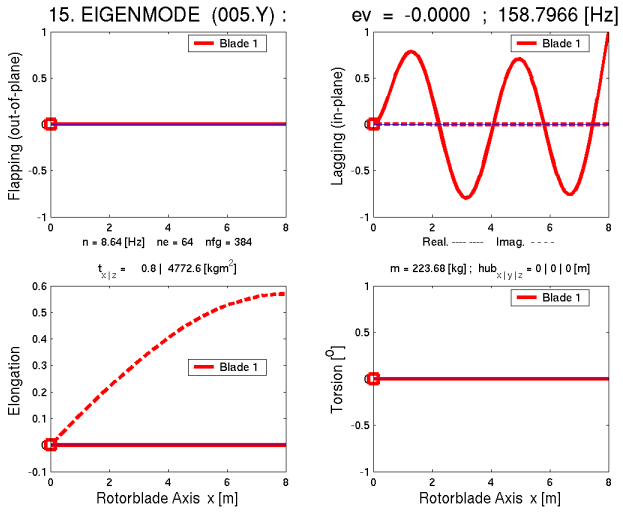

Figure 13: The single blade: The fifth lagging eigenmode at n=8.64[Hz] (GYRBLAD)

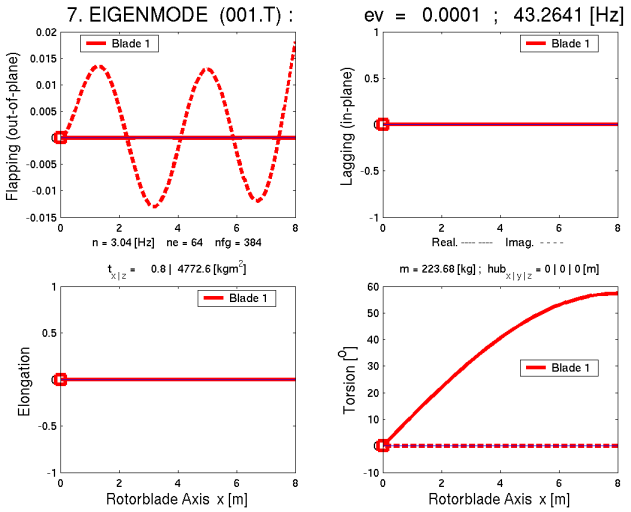

Figure 11: The single blade: The first torsion eigenmode at n=3.04[Hz] (GYRBLAD)

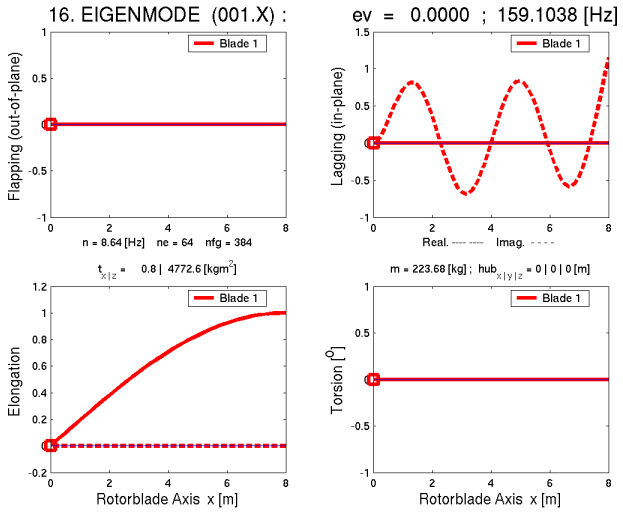

Figure 14: The single blade: The first elongation eigenmode at n=8.64[Hz] (GYRBLAD)

SINGLE BLADE - CLAMPED (32 Elements/Bodies)

n = 0 [Hz]	GYRBLAD (FEM)	SIMPACK (MBS)		SIMPACK/ NASTRAN (FEMBS)	
1.) 1. Flapping ---	0.6392 [Hz]	0.6394 [Hz]	0.03 [%]	0.6392 [Hz]	0.00 [%]
2.) 1. Lagging ---	2.5566 [Hz]	2.5572 [Hz]	0.02 [%]	2.5559 [Hz]	-0.03 [%]
3.) 2. Flapping ---	4.0057 [Hz]	4.0088 [Hz]	0.08 [%]	4.0053 [Hz]	-0.01 [%]
4.) 3. Flapping ---	11.2154 [Hz]	11.2296 [Hz]	0.13 [%]	11.2123 [Hz]	-0.03 [%]
5.) 2. Lagging ---	16.0103 [Hz]	16.0227 [Hz]	0.08 [%]	15.9807 [Hz]	-0.18 [%]
6.) 4. Flapping ---	21.9754 [Hz]	22.0144 [Hz]	0.18 [%]	21.9643 [Hz]	-0.05 [%]
7.) 5. Flapping ---	36.3226 [Hz]	36.4042 [Hz]	0.22 [%]	36.2934 [Hz]	-0.08 [%]
8.) 1. Torsion ---	43.1738 [Hz]	43.1652 [Hz]	-0.02 [%]	43.1752 [Hz]	0.00 [%]
9.) 3. Lagging ---	44.7771 [Hz]	44.8335 [Hz]	0.13 [%]	44.5815 [Hz]	-0.44 [%]
10.) 6. Flapping ---	54.2521 [Hz]	54.3979 [Hz]	0.27 [%]	54.1889 [Hz]	-0.12 [%]
11.) 7. Flapping ---	75.7624 [Hz]	75.9952 [Hz]	0.31 [%]	75.6421 [Hz]	-0.16 [%]
12.) 4. Lagging ---	87.5968 [Hz]	87.7485 [Hz]	0.17 [%]	86.8985 [Hz]	-0.80 [%]
13.) 8. Flapping ---	100.8521 [Hz]	101.1930 [Hz]	0.34 [%]	100.6436 [Hz]	-0.21 [%]
14.) 9. Flapping ---	129.5210 [Hz]	129.9846 [Hz]	0.36 [%]	129.1842 [Hz]	-0.26 [%]
15.) 2. Torsion ---	129.6255 [Hz]	129.3915 [Hz]	-0.18 [%]	129.6295 [Hz]	0.00 [%]
16.) 5. Lagging ---	144.4883 [Hz]	144.7980 [Hz]	0.21 [%]	142.6794 [Hz]	-1.25 [%]
17.) 1. Elongation ---	158.2980 [Hz]	158.2664 [Hz]	-0.02 [%]	158.2980 [Hz]	0.00 [%]

Table 7: The eigenfrequencies of the clamped non-rotating single blade (n=0[Hz]) (three methods FEM, MBS, FEMBS; errors related to the FEM solution)

ISOLATED ROTOR - ELASTIC HUB (4x32 Elements/Bodies)

n = 0 [Hz]	GYRBLAD (FEM)	SIMPACK (MBS)		SIMPACK/ NASTRAN (FEMBS)	
1.) 1. Flapping 0 K ---	0.6391 [Hz]	0.6393 [Hz]	0.03 [%]	0.6391 [Hz]	0.00 [%]
2.) 1. Flapping 1 K ---	0.6391 [Hz]	0.6393 [Hz]	0.03 [%]	0.6391 [Hz]	0.00 [%]
3.) 1. Flapping 1 K ---	0.6391 [Hz]	0.6393 [Hz]	0.03 [%]	0.6391 [Hz]	0.00 [%]
4.) 1. Flapping 2 K ---	0.6392 [Hz]	0.6394 [Hz]	0.03 [%]	0.6392 [Hz]	0.00 [%]
5.) 1. Lagging 1 K ---	2.5501 [Hz]	2.5507 [Hz]	0.02 [%]	2.5495 [Hz]	-0.02 [%]
6.) 1. Lagging 1 K ---	2.5501 [Hz]	2.5507 [Hz]	0.02 [%]	2.5495 [Hz]	-0.02 [%]
7.) 1. Lagging 0 K ---	2.5533 [Hz]	2.5539 [Hz]	0.02 [%]	2.5527 [Hz]	-0.02 [%]
8.) 1. Lagging 2 K ---	2.5566 [Hz]	2.5572 [Hz]	0.02 [%]	2.5559 [Hz]	-0.03 [%]
9.) 2. Flapping 0 K ---	3.9990 [Hz]	4.0021 [Hz]	0.08 [%]	3.9985 [Hz]	-0.01 [%]
10.) 2. Flapping 1 K ---	4.0052 [Hz]	4.0083 [Hz]	0.08 [%]	4.0048 [Hz]	-0.01 [%]
11.) 2. Flapping 1 K ---	4.0052 [Hz]	4.0083 [Hz]	0.08 [%]	4.0048 [Hz]	-0.01 [%]
12.) 2. Flapping 2 K ---	4.0057 [Hz]	4.0088 [Hz]	0.08 [%]	4.0053 [Hz]	-0.01 [%]
13.) 3. Flapping 0 K ---	11.1641 [Hz]	11.1785 [Hz]	0.13 [%]	11.1611 [Hz]	-0.03 [%]
14.) 3. Flapping 1 K ---	11.2140 [Hz]	11.2282 [Hz]	0.13 [%]	11.2109 [Hz]	-0.03 [%]
15.) 3. Flapping 1 K ---	11.2140 [Hz]	11.2282 [Hz]	0.13 [%]	11.2109 [Hz]	-0.03 [%]
16.) 3. Flapping 2 K ---	11.2154 [Hz]	11.2296 [Hz]	0.13 [%]	11.2123 [Hz]	-0.03 [%]
17.) 2. Lagging 1 K ---	15.3140 [Hz]	15.3254 [Hz]	0.07 [%]	15.2880 [Hz]	-0.17 [%]
18.) 2. Lagging 1 K ---	15.3140 [Hz]	15.3254 [Hz]	0.07 [%]	15.2880 [Hz]	-0.17 [%]
19.) 2. Lagging 0 K ---	15.9900 [Hz]	16.0024 [Hz]	0.08 [%]	15.9606 [Hz]	-0.18 [%]
20.) 2. Lagging 2 K ---	16.0103 [Hz]	16.0227 [Hz]	0.08 [%]	15.9807 [Hz]	-0.18 [%]
21.) 4. Flapping 0 K ---	21.7740 [Hz]	21.8137 [Hz]	0.18 [%]	21.7630 [Hz]	-0.05 [%]
22.) 4. Flapping 1 K ---	21.9727 [Hz]	22.0116 [Hz]	0.18 [%]	21.9616 [Hz]	-0.05 [%]
23.) 4. Flapping 1 K ---	21.9727 [Hz]	22.0116 [Hz]	0.18 [%]	21.9616 [Hz]	-0.05 [%]
24.) 4. Flapping 2 K ---	21.9754 [Hz]	22.0144 [Hz]	0.18 [%]	21.9643 [Hz]	-0.05 [%]
25.) 3p Lagging 1 K ---	26.4187 [Hz]	26.4178 [Hz]	-0.00 [%]	26.4182 [Hz]	-0.00 [%]
26.) 3p Lagging 1 K ---	26.4187 [Hz]	26.4178 [Hz]	-0.00 [%]	26.4182 [Hz]	-0.00 [%]
27.) 5. Flapping 0 K ---	35.7486 [Hz]	35.8342 [Hz]	0.24 [%]	35.7202 [Hz]	-0.08 [%]
28.) 5. Flapping 1 K ---	36.3181 [Hz]	36.3996 [Hz]	0.22 [%]	36.2889 [Hz]	-0.08 [%]
29.) 5. Flapping 1 K ---	36.3181 [Hz]	36.3996 [Hz]	0.22 [%]	36.2889 [Hz]	-0.08 [%]
30.) 5. Flapping 2 K ---	36.3226 [Hz]	36.4042 [Hz]	0.22 [%]	36.2934 [Hz]	-0.08 [%]
31.) 1. Torsion 1 K ---	43.1701 [Hz]	43.1618 [Hz]	-0.02 [%]	43.1718 [Hz]	0.00 [%]
32.) 1. Torsion 1 K ---	43.1703 [Hz]	43.1618 [Hz]	-0.02 [%]	43.1718 [Hz]	0.00 [%]
33.) 1. Torsion 2 K ---	43.1725 [Hz]	43.1652 [Hz]	-0.02 [%]	43.1752 [Hz]	0.01 [%]
34.) 1. Torsion 0 K ---	43.1725 [Hz]	43.1652 [Hz]	-0.02 [%]	43.1752 [Hz]	0.01 [%]
35.) 3. Lagging 0 K ---	44.7207 [Hz]	44.7767 [Hz]	0.13 [%]	44.5262 [Hz]	-0.43 [%]
36.) 3. Lagging 2 K ---	44.7771 [Hz]	44.8335 [Hz]	0.13 [%]	44.5815 [Hz]	-0.44 [%]
37.) 3. Lagging 1 K ---	46.4862 [Hz]	46.5331 [Hz]	0.10 [%]	46.3057 [Hz]	-0.39 [%]
38.) 3. Lagging 1 K ---	46.4862 [Hz]	46.5331 [Hz]	0.10 [%]	46.3057 [Hz]	-0.39 [%]

Table 8: The eigenfrequencies of the non-rotating 4-blade-rotor (with c_i =20/20/30/40/40/50[Hz], n=0[Hz]) (three methods FEM, MBS, FEMBS; errors related to the FEM solution)

SINGLE BLADE - CLAMPED (32 Elements/Bodies)

n = 6 [Hz]	GYRBLAD (FEM)	SIMPACK (MBS)		SIMPACK/ NASTRAN (FEMBS)	
1.) 1. Lagging ---	3.4146 [Hz]	3.4219 [Hz]	0.21 [%]	3.4083 [Hz]	-0.18 [%]
2.) 1. Flapping ---	6.1988 [Hz]	6.2115 [Hz]	0.20 [%]	6.1979 [Hz]	-0.01 [%]
3.) 2. Flapping ---	15.5739 [Hz]	15.6052 [Hz]	0.20 [%]	15.5708 [Hz]	-0.02 [%]
4.) 2. Lagging ---	21.2790 [Hz]	21.3044 [Hz]	0.12 [%]	21.2653 [Hz]	-0.06 [%]
5.) 3. Flapping ---	26.9831 [Hz]	27.0788 [Hz]	0.35 [%]	26.9791 [Hz]	-0.01 [%]
6.) 4. Flapping ---	41.2738 [Hz]	41.4999 [Hz]	0.55 [%]	41.2660 [Hz]	-0.02 [%]
7.) 1. Torsion ---	43.5402 [Hz]	43.5316 [Hz]	-0.02 [%]	43.5885 [Hz]	0.11 [%]
8.) 3. Lagging ---	51.0314 [Hz]	51.1290 [Hz]	0.19 [%]	50.8861 [Hz]	-0.28 [%]
9.) 5. Flapping ---	58.3910 [Hz]	58.8210 [Hz]	0.74 [%]	58.3813 [Hz]	-0.02 [%]
10.) 6. Flapping ---	78.4173 [Hz]	79.1339 [Hz]	0.91 [%]	78.3905 [Hz]	-0.03 [%]
11.) 4. Lagging ---	94.4371 [Hz]	94.6720 [Hz]	0.25 [%]	93.8408 [Hz]	-0.63 [%]
12.) 7. Flapping ---	101.5047 [Hz]	102.5951 [Hz]	1.07 [%]	101.4436 [Hz]	-0.06 [%]
13.) 8. Flapping ---	127.7888 [Hz]	129.3398 [Hz]	1.21 [%]	127.6655 [Hz]	-0.10 [%]
14.) 2. Torsion ---	129.7480 [Hz]	129.5144 [Hz]	-0.18 [%]	130.6770 [Hz]	0.72 [%]
15.) 5. Lagging ---	151.6450 [Hz]	152.0939 [Hz]	0.30 [%]	150.0096 [Hz]	-1.08 [%]
16.) 9. Flapping ---	157.3732 [Hz]	159.4665 [Hz]	1.33 [%]	157.1578 [Hz]	-0.14 [%]
17.) 1. Elongation ---	158.6410 [Hz]	158.6094 [Hz]	-0.02 [%]	158.6409 [Hz]	-0.00 [%]

Table 9: The eigenfrequencies of the clamped rotating single blade (n=6[Hz]) (three methods FEM, MBS, FEMBS; errors related to the FEM solution)

ISOLATED ROTOR - ELASTIC HUB (4x32 Elements/Bodies)

n = 6 [Hz]	GYRBLAD (FEM)	SIMPACK (MBS)		SIMPACK/ NASTRAN (FEMBS)	
1.) 1. Lagging 1 K ---	2.5242 [Hz]	2.5312 [Hz]	0.28 [%]	2.5190 [Hz]	-0.21 [%]
2.) 1. Lagging 0 K ---	3.4067 [Hz]	3.4140 [Hz]	0.21 [%]	3.4005 [Hz]	-0.18 [%]
3.) 1. Lagging 1 K ---	3.4091 [Hz]	3.4166 [Hz]	0.22 [%]	3.4026 [Hz]	-0.19 [%]
4.) 1. Lagging 2 K ---	3.4146 [Hz]	3.4219 [Hz]	0.21 [%]	3.4083 [Hz]	-0.18 [%]
5.) 1. Flapping 0 K ---	6.1048 [Hz]	6.1172 [Hz]	0.20 [%]	6.1040 [Hz]	-0.01 [%]
6.) 1. Flapping 1 K ---	6.1985 [Hz]	6.2112 [Hz]	0.20 [%]	6.1976 [Hz]	-0.01 [%]
7.) 1. Flapping 1 K ---	6.1985 [Hz]	6.2112 [Hz]	0.20 [%]	6.1976 [Hz]	-0.01 [%]
8.) 1. Flapping 2 K ---	6.1988 [Hz]	6.2115 [Hz]	0.20 [%]	6.1979 [Hz]	-0.01 [%]
9.) 2. Flapping 0 K ---	15.3340 [Hz]	15.3639 [Hz]	0.19 [%]	15.3309 [Hz]	-0.02 [%]
10.) 2. Flapping 1 K ---	15.5732 [Hz]	15.6044 [Hz]	0.20 [%]	15.5701 [Hz]	-0.02 [%]
11.) 2. Flapping 1 K ---	15.5732 [Hz]	15.6044 [Hz]	0.20 [%]	15.5701 [Hz]	-0.02 [%]
12.) 2. Flapping 2 K ---	15.5739 [Hz]	15.6052 [Hz]	0.20 [%]	15.5708 [Hz]	-0.02 [%]
13.) 2. Lagging 1 K ---	17.7189 [Hz]	17.7313 [Hz]	0.07 [%]	17.7013 [Hz]	-0.10 [%]
14.) 2. Lagging 1 K ---	20.8721 [Hz]	20.8948 [Hz]	0.11 [%]	20.8636 [Hz]	-0.04 [%]
15.) 2. Lagging 0 K ---	21.2592 [Hz]	21.2844 [Hz]	0.12 [%]	21.2458 [Hz]	-0.06 [%]
16.) 2. Lagging 2 K ---	21.2790 [Hz]	21.3044 [Hz]	0.12 [%]	21.2653 [Hz]	-0.06 [%]
17.) 3. Flapping 0 K ---	26.4412 [Hz]	26.5306 [Hz]	0.34 [%]	26.4375 [Hz]	-0.01 [%]
18.) 3. Flapping 1 K ---	26.9815 [Hz]	27.0769 [Hz]	0.35 [%]	26.9775 [Hz]	-0.01 [%]
19.) 3. Flapping 1 K ---	26.9815 [Hz]	27.0770 [Hz]	0.35 [%]	26.9776 [Hz]	-0.01 [%]
20.) 3. Flapping 2 K ---	26.9831 [Hz]	27.0788 [Hz]	0.35 [%]	26.9791 [Hz]	-0.01 [%]
21.) 3p Lagging 1 K ---	29.4375 [Hz]	29.4417 [Hz]	0.01 [%]	29.4504 [Hz]	0.04 [%]
22.) 3p Lagging 1 K ---	29.5874 [Hz]	29.5889 [Hz]	0.01 [%]	29.5893 [Hz]	0.01 [%]
23.) 4. Flapping 0 K ---	40.2024 [Hz]	40.4091 [Hz]	0.51 [%]	40.1948 [Hz]	-0.02 [%]
24.) 4. Flapping 1 K ---	41.2709 [Hz]	41.4966 [Hz]	0.55 [%]	41.2630 [Hz]	-0.02 [%]
25.) 4. Flapping 1 K ---	41.2710 [Hz]	41.4966 [Hz]	0.55 [%]	41.2635 [Hz]	-0.02 [%]
26.) 4. Flapping 2 K ---	41.2738 [Hz]	41.4999 [Hz]	0.55 [%]	41.2660 [Hz]	-0.02 [%]
27.) 1. Torsion 1 K ---	43.5368 [Hz]	43.5282 [Hz]	-0.02 [%]	43.5842 [Hz]	0.11 [%]
28.) 1. Torsion 1 K ---	43.5369 [Hz]	43.5283 [Hz]	-0.02 [%]	43.5853 [Hz]	0.11 [%]
29.) 1. Torsion 0 K ---	43.5402 [Hz]	43.5316 [Hz]	-0.02 [%]	43.5884 [Hz]	0.11 [%]
30.) 1. Torsion 2 K ---	43.5402 [Hz]	43.5316 [Hz]	-0.02 [%]	43.5885 [Hz]	0.11 [%]
31.) 3. Lagging 0 K ---	50.9765 [Hz]	51.0732 [Hz]	0.19 [%]	50.8324 [Hz]	-0.28 [%]
32.) 3. Lagging 2 K ---	51.0314 [Hz]	51.1290 [Hz]	0.19 [%]	50.8861 [Hz]	-0.28 [%]
33.) 3. Lagging 1 K ---	52.1496 [Hz]	52.2404 [Hz]	0.17 [%]	52.0171 [Hz]	-0.25 [%]
34.) 3. Lagging 1 K ---	53.4968 [Hz]	53.5838 [Hz]	0.16 [%]	53.3627 [Hz]	-0.25 [%]
35.) 5. Flapping 0 K ---	56.4419 [Hz]	56.8220 [Hz]	0.67 [%]	56.4341 [Hz]	-0.01 [%]
36.) 5. Flapping 1 K ---	58.3865 [Hz]	58.8158 [Hz]	0.74 [%]	58.3768 [Hz]	-0.02 [%]
37.) 5. Flapping 1 K ---	58.3865 [Hz]	58.8158 [Hz]	0.74 [%]	58.3769 [Hz]	-0.02 [%]
38.) 5. Flapping 2 K ---	58.3910 [Hz]	58.8210 [Hz]	0.74 [%]	58.3813 [Hz]	-0.02 [%]

Table 10: The eigenfrequencies of the rotating 4-blade-rotor (with c_i =20/20/30/40/40/50[Hz], n=6[Hz]) (three methods FEM, MBS, FEMBS; errors related to the FEM solution)

7 The complete isolated rotor

To demonstrate the capability of the MBS code SIMPACK and the FEM code GYRBLAD in predicting the dynamic behaviour of complete rotating rotors the impact of rotation on the eigenmodes and eigenfrequencies of totally elastic rotors has been studied. In the investigation of the complete rotor (four and six blades) all classes of rotor eigenmodes (collective, cyclic and reactionless) had to be distinguished. As results for the eigenbehaviour the coupled complex eigenmodes and the variation of the eigenfrequencies with respect to the rotation speed are shown in a fan diagram (see Fig. 19). The analysed rotors have been built up by the required number of the prior investigated single Princeton blade. Several different rotor systems have been investigated. Beside the rotor speed the main system parameters had been the number of blades, the (mounting) stiffness of the hub and optionally a vertical offset of the mounting point, i.e. the length of the shaft.

In two comprehensive studies for both the non-rotating system and the rotor at the rotation speed of 6 [Hz] the eigenfrequencies of the four blade rotor are presented in a quantifying numerical comparison between the respective eigenmodes. The results for the case of a stiff hub (c_i = 20/20/30/40/40/50 [Hz]) are shown in the Tab. 8 and 10. (the c_i-values denominate the mounting stiffness at the hub for the six DOF at the MBS joint/FEM node for the virtual case of rigid body movement in direction of the respective single DOF.) Like for the single blade the three methods FEM (GYRBLAD), MBS (SIMPACK) and FEMBS (SIMPACK/NASTRAN) had been applied. The error margins proved to be as excellent as in the single blade cases.

Further the results for two selected eigenmodes of the six blade rotor with its even larger variety of rotor modes (one additional 2-node and one 3-node eigenmode for each mode order) are presented. The rotor had been mounted to a stiff hub (c_i = 20/20/30/40/40/50 [Hz]) and the hub node (= shaft height) had an offset of 2 [m]. At a rotation speed of 2 [Hz] the second 1K regressive flapping eigenmode (see Fig. 15 and 16) and the first 1K regressive lagging eigenmode (see Fig. 17 and 18) calculated with SIMPACK as well as with GYRBLAD are shown. In the diagrams of the GYRBLAD results it easily can be perceived that due to the gyroscopic coupling and the displacement of the hub now in contrast to the two blade rotor the eigenmodes consist of all four main deflection components.

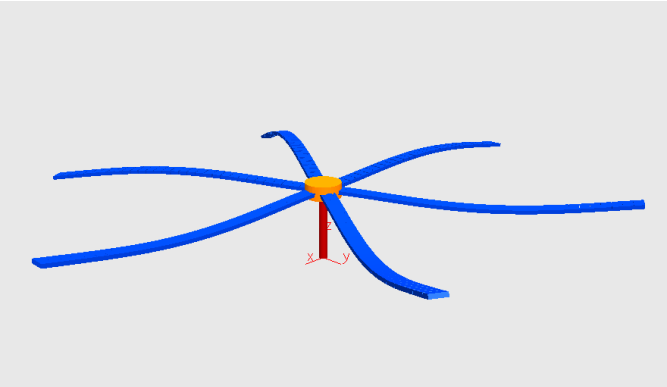

Figure 15: The 6-blade-rotor: The second 1K regressive flapping eigenmode (with f=6.47[Hz], n=2[Hz]) (SIMPACK)

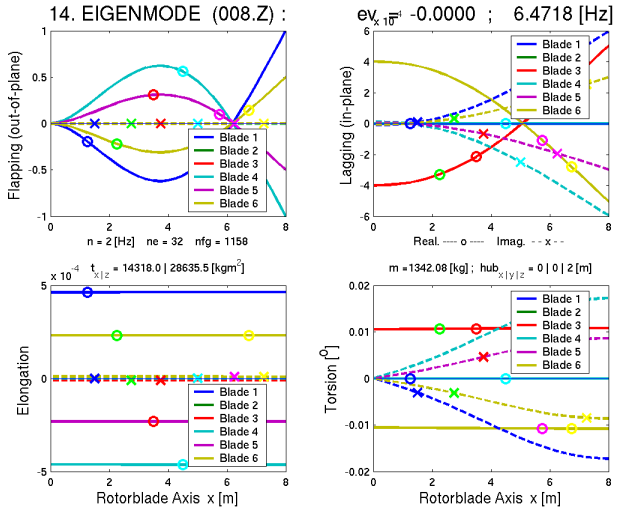

Figure 16: The 6-blade-rotor: The second 1K regressive flapping eigenmode (with f=6.47[Hz], n=2[Hz]) (GYRBLAD)

Finally results are presented for the four blade rotor with a low hub stiffness (c_i = 2/2/3/4/4/5 [Hz]). The eigenfrequencies with respect to rotor speed are shown in the Fig. 19 in a fan diagram at varying rotation speeds up to 5.5 [Hz] as a numerical comparison between the methods GYRBLAD (32 element FEM blade) and SIMPACK (32 rigid

body MBS blade). Also here the SIMPACK results for a selection of distict rotor speeds, denominated with a "x" marker in the diagram, lie exactly on the GYRBLAD curves.

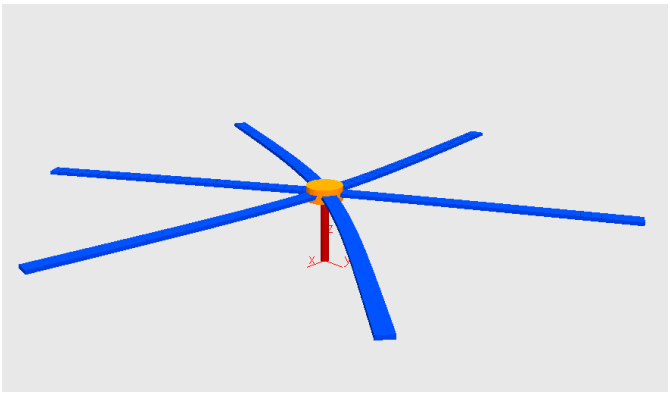

Figure 17: The 6-blade-rotor: The first 1K regressive lagging eigenmode (with f=2.69[Hz], n=2[Hz]) (SIMPACK)

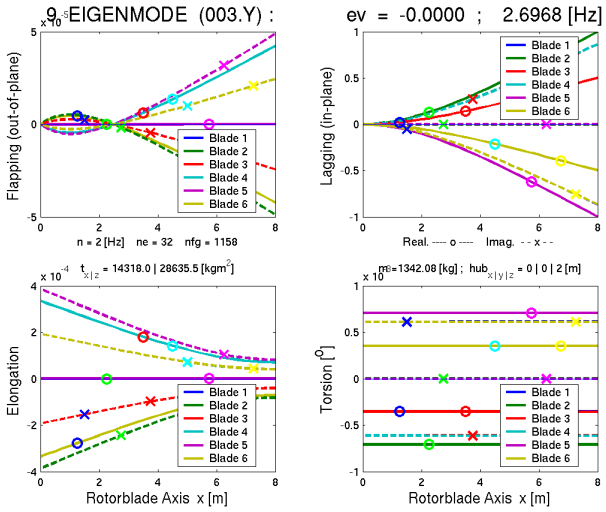

Figure 18: The 6-blade-rotor: The first 1K regressive lagging eigenmode (with f=2.69[Hz], n=2[Hz]) (GYRBLAD)

In all analysed cases the rotor specific features of the eigenbehaviour can well be demonstrated: The eigenmodes can be classified into the mode groups of collective, cyclic and reactionless movement of the blades referring to the number of node diameters (denoted with a "K" in Tab. 8 and 10 together with the counter of the node diameters). The double frequencies of the 1K-cases in non-rotating state are split up with increasing rotor speed, with one frequency branch primarily less increasing than the other or even decreasing. Last not least passing the critical rotation speed the instability case of ground resonance is delivered automatically as a "part of the bargain". In the diagram the stability limit can be found at the place where the eigenfrequencies of the two lower 1K-lagging modes ("01.Y1" and "02.Y1", both in regressive regime now) coalesce again at around 4.5 [Hz] rotor speed (see Fig. 19). In the coalescence point and beyond the solution of the eigenvalue problem renders one of the two 1K-eigenmodes with eigenvalues having positive real parts (the other one with negative real parts).

8 Conclusions

The main topics of this investigation have been:

- Modelling rotating blades and complete elastic rotors with advanced CSD tools like the MBS code SIMPACK,
- studying the impact of rotation on the dynamic behaviour of the elastic structure and
- validating the results of eigenvalue analysis by comparing them with results produced with different methods and other independent codes.

The analysis covered the rotating 8 [m] modified Princeton blade and various full elastic four and six blade rotors with different hub mounting conditions. For the computation of the eigenbehaviour it had been made use of the in-house FEM code GYRBLAD, both the rigid body and the elastic import features of the MBS code SIMPACK (combined with NASTRAN beam models) and last but not least analytical models of few degree of freedom rotors.

Concerning the physical aspects the aim has been the modelling of the complete gyroscopic and stiffening terms necessary to map the linear stability behaviour of the rotating structure. The focus was put on the coupling mechanism between the degrees of freedom by the influence of the rotatory movement.

With the analysed blade areas of rotation speed have been detected where the structure is extremely

prone to gyroscopic interaction between the components of deformation from which the torsional deflection in terms of aeroelasticity seems to be the most relevant. Such gyroscopic resonance phenomena can be hazardous to flight safety since together with the aerodynamic forces acting on the blades they might enlarge the affinity of the rotor for aeroelastic instability.

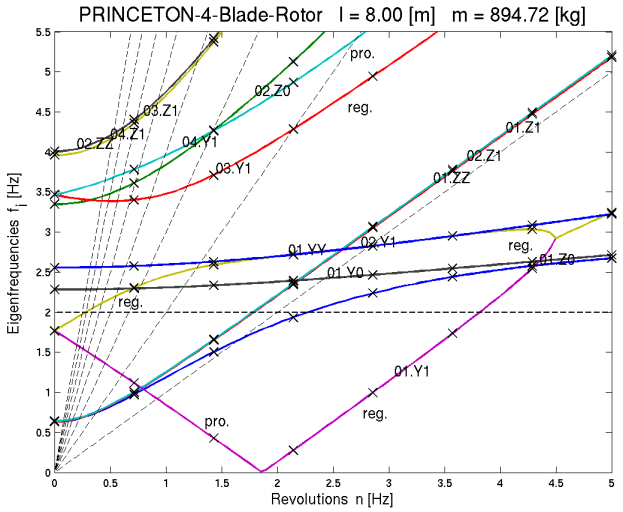

Figure 19: The 4-blade-rotor: The lower eigenfrequencies w/r to rotor speed ($c_y = c_z = 2$[Hz]) (GYRBLAD; × = SIMPACK)

Finally for validation purposes the results of the MBS code have been compared quantitatively to the results gained with the other methods presented. The MBS results for the eigenfrequencies proved their compliance up to the numerical model accuracy (in the promille error range). Thus the potential of a sophisticated, hybrid MBS code like SIMPACK as a powerful simulation tool for helicopter dynamics has been demonstrated with respect to the structural dynamics of the elastic rotor.

9 Symbols

u, v, w	Displacements of the beam cross sectional centre of gravity
α, β, γ	Rotations of the beam cross section
x, y, z	Coordinates of the beam, with x being the longitudinal beam axis
l_k, b, h	Dimensions of each of the rigid bodies of the double pendulum
l_g	Total length of the double pendulum
m	Total mass of the double pendulum
η	Prandtl torsional coefficient ($\eta \to 1$ with $b/h \to \infty$)
n	Number of revolutions of the rotor
μ_x	Transversal mass distribution of the beam
$\widehat{\mu}_h$	Rotational mass distribution of the beam

References

[1] Hopkins, A. Stewart; Ormiston, Robert A.: *An Examination of Selected Problems in Rotor Blade Structural Mechanics and Dynamics.* American Helicopter Society, 59th Annual Forum, Phoenix, Az., May 6. – 8. 2003.

[2] Gasch, Robert; Knothe, Klaus: *Strukturdynamik.* Vol. 1 and 2, Springer-Verlag Berlin, 1989.

[3] Fa. INTEC GmbH/SIMPACK AG: *SIMPACK Reference Guide and SIMDOC Manuals.* Vers. 8805 (8900), Munich, 8. Sept. 2007

[4] Johnson, Wayne: *Helicopter Theory.* Dover Publications, Inc., New York, 1994.

[5] Bielawa, Richard L.: *Rotary Wing Structural Dynamics and Aeroelasticity.* AIAA Educational Series, American Institute of Aeronautics and Astronautics, Wash., 1992.